COBEM 2023 27TH INTERNATIONAL CONGRESS OF MECHANICAL ENGINEERING

ABCM Brazilian Society of Mechanical Sciences and Engineering
27th ABCM International Congress of Mechanical Engineering
December 04-08, 2023, Florianópolis-SC, Brazil

# COB-2023-0144
# SIMULATION OF HYPERSONIC FLOWS IN THERMOCHEMICAL NON-EQUILIBRIUM CONDITIONS: INFLUENCE OF THE CONTROL TEMPERATURE OF PARK'S TWO-TEMPERATURE MODEL IN THE FLOW BEHAVIOR

**Gibson De Marchi Poltronieri**
**Farney Coutinho Moreira**
Instituto Tecnológico de Aeronáutica, ITA, 12228-900, São José dos Campos, SP, Brazil
gibsondemarchi@gmail.com
farney.coutinho@gmail.com

**João Luiz F. Azevedo**
Instituto de Aeronáutica e Espaço, DCTA/IAE, 12228-904, São José dos Campos, SP, Brazil
joaoluiz.azevedo@gmail.com

***Abstract.*** *Numerical simulations of hypersonic flows under thermochemical non-equilibrium conditions are presented for the FIRE II capsule. An 11-species model is used to describe the flow gas mixture. The present work analyzes the influence of the control temperature weight factors in Park's two-temperature model on the flow behavior. The analysis performed aims to broaden the understanding of the weight factors influence. The work uses a code developed for solving the Navier-Stokes equations and Park's model using a finite volume approach. The work presents results in terms of the Mach number and temperature modes along the stagnation streamline. In addition, this work includes results for the heat flux at the stagnation point. The change in the weight factors leads to changes in the maximum temperature values, the shock wave position, and the flow gas composition. The heat flux at the stagnation point does not change significantly in the analysis performed. The results are in good agreement with experimental data. The present work indicates that the weight factors in Park's two-temperature model can have a rather significant effect on the position of the shock wave and behavior of the flow non-equilibrium region.*

***Keywords:*** *Hypersonic Flow, CFD, Thermodynamic non-equilibrium, Chemical non-equilibrium, Temperature Models.*

## 1. INTRODUCTION

Public agencies and private organizations started to grow interested in aerospace exploration. The reentry procedure plays a critical role in space missions to guarantee the safety and integrity of the vehicle and payload. The hypersonic vehicle achieves high speeds during the atmospheric entry/reentry procedure. As the body enters a high-density part of the atmosphere, the complexity of the flow increase. Near the vehicle body occur the formation of a high-temperature shock layer. High-temperature gas phenomena, such as thermodynamic and chemical non-equilibrium, become more present. Dissociation, recombination, and ionization chemical reactions occur in these conditions, changing the flow gas mixture composition. These complex phenomena lead to the excitation of different energy modes. The high-temperature and reacting gas mixture conditions affect the reentry vehicle and capsule thermal protection system (TPS).

The present work studies the influence of the weight factors of the control temperature calculation of Park's two-temperature model on flow behavior. The study uses three points of the descended trajectory of the FIRE II capsule. The simulation results are obtained with the improved LeMANS code and compared with existing data in the literature. The results presented in this work consider only convective effects. The experimental data used for the comparison includes both convective and radiative effects (Johnston *et al.*, 2008).

The thermal protection system of the FIRE II capsule has three thermal shields. The first shield, with radius $R_n = 934.70$ mm, protects the capsule until an altitude of approximately 60 km, then it is ejected. The second shield, with radius $R_n = 805.20$ mm, stays active until an altitude of approximately 45 km. The end of the reentry procedure uses the third shield with a radius $R_n = 702.00$ mm. The present work analysis uses one case from each thermal shield. Moreira *et al.* (2021) show a detailed image of the geometry of the FIRE II capsule.

Uncertainties arise from the use of numerical methods and models. In computational fluid dynamics (CFD), the validation of the results from the simulations is of utmost importance. Furthermore, an understanding of the influence of numerical parameters is also necessary. The present work compares its results with the aerothermodynamic data obtained from Cornette (1966). The computations performed considered a freestream gas mixture with 11 species that simulate

the atmosphere of the Earth. The present work assumes an initial gas mixture mass composition of 76.30% of molecular nitrogen and 23.70% of molecular oxygen.

The weight factors chosen encompass those regarded as good choices by the literature. The present work presents results for the Mach number and temperature modes along the stagnation line for each weight factor value chosen, focusing on the non-equilibrium region. In addition, this work includes results for the heat flux at the stagnation point. With this analysis, the present work aims to broaden the knowledge about the influence of the Park's two temperature model weight factors on the flow behavior.

## 2. THEORETICAL FORMULATION

### 2.1 General Considerations

The density of the freestream flow varies with the altitude. Thus the reentry vehicle or capsule experience different types of flow regimes in its reentry trajectory. Depending on the flow regime, some formulations are not valid. The Knudsen number is a dimensionless parameter that defines the flow as a continuum or rarefied medium, written as

$$Kn = \frac{\lambda}{L} \quad , \tag{1}$$

where $\lambda$ is the mean free path, in other words, the average distance that a particle travels until colliding with another. In this case, the particle is either an atom or a molecule. The parameter $L$ is the characteristic length which is a representative measure of the dimension of the fluid-immersed object (Bird, 1994).

For reentry capsules, the characteristic length is usually the outer radius or the outer diameter. Flow properties, such as pressure, temperature, density, Reynolds Number, and Mach number, define the freestream flow in a continuum formulation, such as Navier-Stokes. Thus, it is interesting to obtain the Knudsen number from these parameters. Considering the hard-sphere model for a particle collision cross section, as presented in Boyd and Schwartzentruber (2017), it is possible to rewrite the Knudsen number as a function of the Reynolds number, Mach number, and ratio of specific heats as

$$Kn = \frac{M}{Re}\sqrt{\frac{\gamma\pi}{2}} \quad . \tag{2}$$

In this expression, $\gamma$ is the ratio of specific heat, $M$ is the Mach number, and $Re$ is the Reynolds number.

For Knudsen number values up to $Kn = 0.01$, the flow is in the continuum regime and the Navier-Stokes equations are valid. The formulation must consider the slip condition for the Knudsen number in the range of $0.001 \leq Kn < 0.01$. The flow regime is transitional if the Knudsen number ranges from $0.01 \leq Kn < 1$. In this regime, the formulation must follow the kinetic theory, such as the Burnett equation (Agarwal *et al.*, 2001). In cases where the Knudsen number is $Kn > 1$, the flow is classified as rarefied. The formulation for these cases uses binary collision models derived from the Boltzmann equation. For Knudsen numbers tending to infinity, $Kn \to \infty$, the flow tends to the free-molecule limit (Bird, 1994; Boyd and Schwartzentruber, 2017). In this case, the formulation considered must be the collisionless Boltzmann equation.

The Direct Simulation Monte Carlo (DSMC) is a collision-based solver for high values of the Knudsen number. Also, the DSMC method can solve regimes with low values of the Knudsen number, but the computational and time resources are very high (Bird, 1994). For the simulations in the present work, the Knudsen number is in the order of magnitude of $10^{-3}$. Thus, the regime flow is a continuum. Hence, the Navier-Stokes constitute an accurate model for the high-enthalpy flows considered in the present work. In addition, to account for thermodynamic non-equilibrium and weak ionization effects, this work solver uses Park's two-temperature model (Park, 1989). This model couples the temperature of the translational and rotational energies into a single temperature defined as $T_{tr}$. The second temperature $T_{ve}$, describes the vibrational and electronic energy modes plus the electron energy (Scalabrin, 2007; Martin *et al.*, 2012).

### 2.2 Conservation Equations and Related Models

Through the Boltzmann equation and the Chapman-Enskog theory, it is possible to obtain the system of conservation equations for mass, momentum, and energy transport, known as the Navier-Stokes equations (Boyd and Schwartzentruber, 2017). In the present analysis, the system of equations contains two source terms. One represents the chemical reactions under thermodynamic non-equilibrium, $S_{cv}$. The other accounts for the axisymmetric flow configuration used in the present work, $S_{axi}$. The Navier-Stokes equations can be written in a multi-dimensional form using the index notation as

$$\frac{\partial Q}{\partial t} + \frac{\partial \left(F_j - F_{v_j}\right)}{\partial x_j} = S_{cv} + S_{axi} \quad , \tag{3}$$

where $Q$ is the vector of conservated variables defined as

$$Q = \left\{\rho_1 \quad \dots \quad \rho_N \quad \rho u_i \quad E \quad E_{ve}\right\}^{\mathsf{T}} \quad . \tag{4}$$

The index notation implies that the free index represents a vectorial equation, and the repeated indices indicate a summation. The density terms $\rho_1, \ \ldots, \ \rho_N$ in the $Q$ vector represent the density of the $N$ chemical species in the gas mixture composition, the term $\rho u_i$ is the macroscopic flow velocity components, $E$ is the total energy per unit volume, and $E_{ve}$ is the energy per unit volume associated with the vibrational-electronic temperature $T_{ve}$.

The inviscid and viscous flux terms, $F_j$ and $F_{v_j}$, respectively, are defined as

$$F_j = \begin{Bmatrix} \rho_1 u_j \\ \vdots \\ \rho_N u_j \\ \rho u_i u_j + p\delta_{ij} \\ (E+p)\, u_j \\ E_{ve} u_j \end{Bmatrix} \quad \text{and} \quad F_{v_j} = \begin{Bmatrix} -J_{1,j} \\ \vdots \\ -J_{N,j} \\ \tau_{ij} \\ \tau_{ij} - (q_{tr,j} + q_{ve,j}) - \sum (J_{s,j} h_s) \\ -q_{ve,j} - \sum (J_{s,j} e_{ve,s}) \end{Bmatrix} \quad . \tag{5}$$

In $F_j$ and $F_{v_j}$, $p$ is the gas mixture pressure, $\delta_{ij}$ is the Kronevker delta, $\tau_{ij}$ represents the viscous stress tensor components, and $J_{s,j}$ is the diffusion flux of the $s$-th chemical species in the $j$-th direction and given by $J_{s,j} = \rho D_s \frac{\partial Y_s}{\partial x_j}$, according to Fick's Law (Bird *et al.*, 2002). In the definition of $J_{s,j}$, $D_s$ is the diffusion coefficient, and $Y_s$ is the molar fraction of the chemical specie $s$. Also, $h_s$ represents the enthalpy of the $s$ specie. The thermal flux $q_{tr,j}$ represents the flux related to the coupled translational-rotational temperature $T_{tr}$ in the $j$-th direction, and $q_{ve,j}$ is the thermal flux associated with the coupled vibrational-electronic temperature $T_{ve}$ in the $j$-th direction.

Assuming that each chemical specie $s$ behave as an ideal gas and Dalton's Law of partial pressures is valid, the gas mixture pressure $p$ is given by

$$p = \sum_{s=1}^{N} \left( \frac{\rho_s R}{M_s} T_{tr} \right) + \frac{\rho_e R}{M_e} T_{ve} \quad , \tag{6}$$

where $R$ is the universal gas constant, $\rho_s$ and $M_s$ are the density and molecular weight of individual species, respectively, $\rho_e$ is the electronic density, and $M_e$ is the electronic molecular weight (Gillespie, 1930).

The viscous stress tensor for a Newtonian fluid is given by

$$\tau_{ij} = \mu \left( \frac{\partial u_i}{\partial x_j} + \frac{\partial u_j}{\partial x_i} \right) - \left( \frac{2}{3}\mu - \beta \right) \frac{\partial u_k}{\partial x_k} \delta_{ij} \quad , \tag{7}$$

where $\mu$ is the shear viscosity and $\beta$ is the bulk viscosity. The bulk viscosity arises from the momentum exchange between colliding molecules and their internal degrees of freedom. The bulk viscosity contributes to the dilatational term that appears in the normal stress. Therefore, $\beta$ could directly impact the momentum exchange observed in the present calculation procedure, especially if the flow gas mixture contains carbon dioxide.

Cramer (2012); Jaeger *et al.* (2018); Sharma and Kumar (2019) presents estimation models for the bulk viscosity under different temperature ranges. However, these models are for low temperatures. Since this topic is still under investigation and the temperatures in the observed flows are high, the present formulation assumes that Stokes' hypothesis is valid, so $\beta = 0$. This assumption aims to avoid inaccuracies in the bulk viscosity evaluation, and this work is primarily concerned with the atmosphere of the Earth.

The current formulation uses Fourier's Law of heat conduction to model the heat fluxes as

$$q_{tr,j} = -\kappa_{tr} \frac{\partial T_{tr}}{\partial x_j} \quad \text{and} \quad q_{ve,j} = -\kappa_{ve} \frac{\partial T_{ve}}{\partial x_j} \quad . \tag{8}$$

Eucken's approach calculates the thermal conductivity of each chemical specie for the translational-rotational and vibrational-electronic energy modes (Vincenti and Kruger, 1982). Thus, $\kappa_{tr,s}$ and $\kappa_{ve,s}$ are given as

$$\kappa_{tr,s} = \mu_s \left( \frac{5}{2} C_{v_{tr,s}} + C_{v_{ve,s}} \right) \quad \text{and} \quad \kappa_{ve,s} = \mu_s C_{v_{ve,s}} \quad , \tag{9}$$

respectively. Here, $C_{v_{tr,s}}$ is the specific heat at constant volume related to the translational-rotational energy mode for the $s$-th chemical specie and the $C_{v_{ve,s}}$ is the specific heat at constant volume related to the vibrational-electronic energy mode for the $s$-th chemical specie.

The present formulation uses Wilke's semi-empirical mixing rule to calculate the gas mixture transport properties (Wilke, 1950). Thus, $\mu$ and $\kappa$ are given by

$$\mu = \sum_s \frac{Y_s \mu_s}{\phi_s} \quad \text{and} \quad \kappa = \sum_s \frac{Y_s \kappa_s}{\phi_s} \quad , \tag{10}$$

respectively. The $\mu_s$ represents the dynamic viscosity for the $s$-th chemical specie, and $\kappa_s$ represents the thermal conductivity coefficients for the $s$-th chemical specie. The term $\phi_s$ is defined by

$$\phi_s = \sum_r Y_r \frac{\left[1 + \sqrt{(\mu_s/\mu_r)}\,(M_r/M_s)^{1/4}\right]^2}{\sqrt{8\,[1 + (M_s/M_r)]}} \quad , \tag{11}$$

where $\mu_r$ is the dynamic viscosity and $M_r$ is the molecular weight of an $r$ chemical specie involved in the binary collision with an $s$ chemical specie (Scalabrin, 2007).

In Eq. (3), the $S_{axi}$ source term represents additional surface stresses that appear from the axisymmetric formulation. The contribution is only to the $y$-momentum equation to counterbalance the pressure and viscous forces acting on the side surfaces of the control volume. Hence, $S_{axi}$ is given by

$$S_{axi} = \left\{0 \quad \ldots \quad 0 \quad \left[-p + 2\mu\left(\frac{u_2}{\bar{x}_2} - \frac{1}{3}\frac{\partial u_k}{\partial x_k}\right)\right]\frac{\delta_{i2}}{\bar{x}_2} \quad 0 \quad 0\right\}^{\mathsf{T}} \quad , \tag{12}$$

where $\bar{x}_2$ is the radial coordinate measured from the axis of symmetry to the cell centroid. For the axisymmetrical flow, the dilatation term is defined by

$$\frac{\partial u_k}{\partial x_k} = \frac{\partial u_1}{\partial x_1} + \frac{\partial u_2}{\partial x_2} + \frac{\partial u_2}{\partial \bar{x}_2} \quad , \tag{13}$$

where $x_1$ and $x_2$ are the axial and radial directions, respectively.

The source term $S_{cv}$, in Eq. (3), represents the rates of mass production of the chemical species from the chemical reactions and given by

$$S_{cv} = \left\{\dot{\omega}_1 \quad \ldots \quad \dot{\omega}_N \quad 0 \quad 0 \quad 0 \quad 0 \quad \dot{\omega}_v\right\}^{\mathsf{T}} \quad , \tag{14}$$

where $\dot{\omega}_v$ is the vibrational energy source term, and the terms $\dot{\omega}_1,\ \ldots,\ \dot{\omega}_N$ represents the mass production rates of the $N$ species due to the chemical reactions.

### 2.3 Chemical Species and Model of Chemical Reactions

Phenomena associated with chemical reactions, such as dissociation, recombination, and ionization, caused by high-enthalpy flows change the flow gas mixture composition. Some chemical models developed aim to represent the high-enthalpy phenomena according to the complexity of the flow physics and chemical reactions (Gnoffo *et al.*, 1989). The present work uses an 11-species model to describe the atmosphere of the Earth. This model considers the species: $N_2$, $O_2$, NO, N, O, $N_2^+$, $O_2^+$, $NO^+$, $N^+$, $O^+$, and $e^-$. Moreira *et al.* (2021) work shows the difference between the 5- and 11-species chemical models on the heat flux at the stagnation point.

The general equation for the dissociation and ionization reactions of the chemical model is described as

$$\sum \alpha_{rs} = \sum \beta_{rs} \quad , \tag{15}$$

where $s$ represents the chemical specie, $\alpha_{rs}$ is the stoichiometric coefficient of the reagents, and $\beta_{rs}$ is the stoichiometric coefficient of the products. To standardize the form of the reactions, they are written so that the right arrow indicates an endothermic reaction. The chemical production rate of the $s$-th specie is given by

$$\dot{\omega}_s = M_s \sum_{r=1}^{nr} (\beta_{rs} - \alpha_{rs}) \left[k_{fr} \prod_{s=1}^{N} \left(\frac{\rho_s}{M_s}\right)^{\alpha_{rs}} - k_{br} \prod_{s=1}^{N} \left(\frac{\rho_s}{M_s}\right)^{\beta_{rs}}\right] \quad , \tag{16}$$

where $k_{fr}$ is the forward reaction rate, and $k_{br}$ is the backward reaction rate.

The $k_{br}$ is defined by the relation of $k_{fr}$ and $k_{br}$ with the equilibrium constant $k_{eq}$ and written as

$$k_{br}(T_c) = k_{fr}(T_c)/k_{eq}(T_c) \quad . \tag{17}$$

The $k_{fr}(T_c)$ values are calculated using Arrhenius curve fits as

$$k_{fr} = A T_c^{\eta_k} \exp\left(-\theta_r/T_c\right) \quad , \tag{18}$$

where $A$ is the pre-exponential factor, $\eta_k$ is the temperature dependence, and $\theta_r$ is the activation energy. The present work uses the forward rate coefficients proposed by Park (1993).

To calculate the values of $k_{eq}(T_c)$, Park (1989) presents a curve fitted polynomial defined as

$$k_{eq} = \exp\left[A_1\left(\frac{T_c}{10^4}\right) + A_2 + A_3 \ln\left(\frac{10^4}{T_c}\right) + A_4\left(\frac{10^4}{T_c}\right) + A_5\left(\frac{10^4}{T_c}\right)^2\right] \quad , \tag{19}$$

where the coefficients $A_1$, $A_2$, $A_3$, $A_4$, and $A_5$ are functions of the flow particle number density within the range of the data tabulated in Park (1989). In cases where the values of number densities are outside de valid range, the formulation uses the maximum and minimum values tabulated accordingly.

The non-equilibrium occurs when the timescale of the flow movement is in the same order of magnitude as the relaxation time required to achieve the equilibrium state. Thus, models considering a finite rate of chemical reactions are appropriate to account for the non-equilibrium effects. A widely used model due to its simplicity is the two-temperature model proposed by Park (1989). Park's model defines the control temperature, $T_c$, used to calculate the forward and equilibrium rates as $T_c = T_{tr}^a T_{ve}^b$, where $a$ and $b = 1 - a$ are the non-equilibrium weight factors that control the energy transfer between dissociation and ionization reactions.

The control temperature $T_c$ combines the coupled temperatures $T_{tr}$ and $T_{ve}$ to control the dissociation reactions. This formulation accounts for the fact that vibrationally excited molecules are more likely to dissociate (Park, 1989). Park (2010) shows that the value o $a$ is taken to be between $0.5$ and $0.7$. Niu *et al.* (2018) presents an analysis for $a = 0.5$ and $a = 0.7$, values considered standard by the literature, and three different chemical models over a blunt body configuration. Also, it shows that the weight factors have a significant role in the distribution of the $T_{ve}$ in the non-equilibrium process.

The present work uses a set of values of $a$ ranging from $0.4$ to $0.8$ by a step of $0.1$, which includes the commonly used values in the literature. Moreover, the work performs the weight factor analyses on three different flow conditions based on instants along the FIRE II reentry trajectory.

## 3. NUMERICAL FORMULATION

The present work uses the LeMANS parallel code developed at the University of Michigan (Scalabrin, 2007). The code solves the Navier-Stokes equations using a finite volume method with a cell-centered approach. Furthermore, LeMANS is capable of axisymmetric flow using meshes composed solely of quadrilaterals to better resolve the boundary layers and shock waves.

The LeMANS code uses a modified Steger-Warming flux vector splitting scheme to discretize the inviscid fluxes across cell faces (MacCormack and Candler, 1989). The method switches to the original Steger-Warming scheme at the shock wave by a pressure switch (Steger and Warming, 1981). The modified version is less dissipative and yields better results along the boundary layer, while the original is more dissipative and better suited for the shock wave. The solver implements a second-order reconstruction of the inviscid fluxes, as presented in Scalabrin (2007).

The code calculates the viscous fluxes using a second-order centered scheme that combines properties at cell centers and nodes. The solver evaluates the values of properties at the nodes using a simple average of the cell values that share the node. This method increases the stencil employed in the derivative calculations, avoiding loss of accuracy in unstructured meshes. The formulation uses a no-slip velocity boundary condition with a catalytic isothermal wall at the solid surfaces for the analyses performed in this work. Moreira *et al.* (2021) present more information about the influence of catalytic and non-catalytic wall conditions.

The spatial discretization of the source term is the same as the one used for the viscous terms. The code calculates values of properties on the left and right sides of a volume face using the value of the respective volume centroid and values of properties of the nodes that compose the control volume (Jawahar and Kamath, 2000). One possible numerical problem associated with the source term is that chemical reaction rates can achieve large values depending on the control volume temperature, especially for low equilibrium constant values, $k_{eq}$ (Park, 1988). Another problem relates to the density of the chemical species, which needs to be positive. Negative values lead to a change of the source term sign, thus numerical instabilities. During the convergence process of the solver, the calculation procedure of the density at a given control volume with a small density value can lead to negative values for some species. To overcome any problems in the source terms calculation, the solver uses a modified temperature to numerically obtain the chemical reaction rates (Scalabrin, 2007).

Numerical instabilities may also appear with explicit methods for the time integration of the Navier-Stokes equations including the source terms. In such cases, the time step restriction due to numerical stiffness does not allow an adequate iteration time to achieve convergence of the solution (Hirsch, 2007). For steady-state solutions, implicit schemes for time integration improve efficiency and robustness. Moreover, it allows for larger time steps while avoiding the growth of numerical instabilities. The solver uses a line implicit method for the time integration (Venkatakrishnan, 1995).

## 4. RESULTS

Freestream conditions used in the simulations are based on experimental data from the FIRE II reentry trajectory and described in Tab. 1. In the referenced table, $t$ is the trajectory time in seconds counted from launch on the ground,

$H$ is the flight altitude, $\rho_\infty$ is the freestream density, $T_\infty$ and $T_w$ are the freestream and FIRE II surface temperatures, respectively, $U_\infty$ is the flow speed, $R_n$ is the radius of the thermal protection, $M_\infty$ is the freestream Mach number, $Re_\infty$ is the reference Reynolds number, and $Kn_\infty$ is the freestream Knudsen number.

Table 1: Freestream flow conditions.

| $t(s)$ | $H(km)$ | $\rho_\infty(kg/m^3)$ | $T_\infty(K)$ | $T_w(K)$ | $U_\infty(m/s)$ | $R_n(m)$ | $M_\infty$ | $Re_\infty$ | $Kn_\infty$ |
|---|---|---|---|---|---|---|---|---|---|
| 1,636 | 71.02 | $8.57 \times 10^{-5}$ | 210 | 810 | 11,310 | 0.935 | 38.85 | $2.19 \times 10^4$ | $2.63 \times 10^{-3}$ |
| 1,645 | 48.37 | $1.32 \times 10^{-3}$ | 285 | 1,520 | 9,830 | 0.805 | 28.99 | $2.17 \times 10^5$ | $1.97 \times 10^{-4}$ |
| 1,648 | 41.60 | $3.25 \times 10^{-3}$ | 267 | 503 | 8,100 | 0.702 | 24.68 | $4.32 \times 10^5$ | $8.46 \times 10^{-5}$ |

### 4.1 Computational Grid

The grids used for the numerical simulations performed in the present work are composed solely of quadrilaterals. The grids made for each thermal shield of the FIRE II have two distinct regions of refinement, one for the thermal shield wall and the other for the non-equilibrium region. The non-equilibrium grid refinement region must include the shock wave and the thermodynamic non-equilibrium immediately behind it. This work defines the non-equilibrium refinement region using the results from Moreira (2020) and Moreira *et al.* (2021). Based on the results from Moreira *et al.* (2023), the present work uses a uniformly refined mesh at the non-equilibrium region with $Re_{cell} \approx 5$ and a stretching factor of $10\%$ for a smooth transition to other mesh regions. The mesh at the vehicle wall uses $Re_{cell} \approx 1$ for the first cell and a stretching factor of $5\%$. Table 2 shows the number of control volumes in the wall-normal and streamwise directions, as well as the total number of grid control volumes for each case analyzed in the present work. Figure 1 represents the meshes used for each condition analyzed in this work. Compared to Moreira *et al.* (2023), the present work mesh refinement drastically increases the number of cells, thus the computational cost. However, the new mesh refinement approach aims to yield better resolution of the flowfield properties in the non-equilibrium region.

Table 2: Mesh parameters.

| $H(km)$ | Wall-normal direction | Streamwise direction | Total |
|---|---|---|---|
| 71.02 | 490 | 148 | 72,520 |
| 48.37 | 739 | 148 | 109,372 |
| 41.60 | 1,130 | 138 | 155,940 |

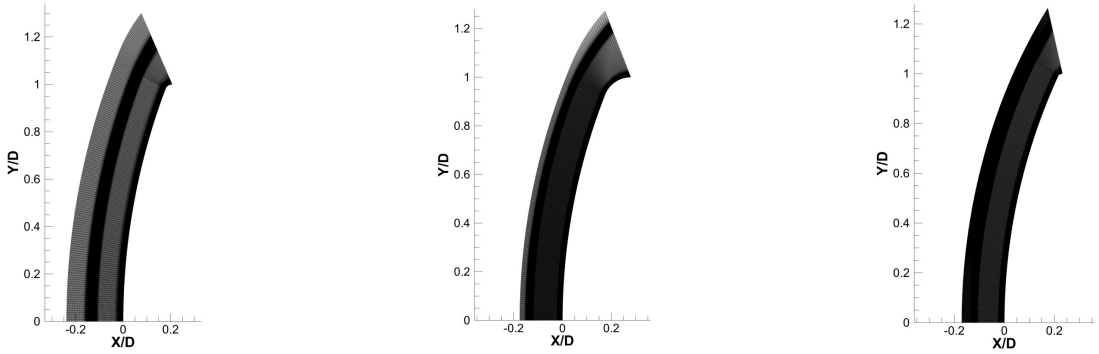


(a) $H = 71.02$ km. (b) $H = 48.37$ km. (c) $H = 41.60$ km.

Figure 1: Computational grids used in the simulations.

### 4.2 Shock Wave Position

Figure 2 shows the Mach number distribution along the stagnation streamline for each condition considered. The results show the expected behavior of the shock wave when compared with Moreira (2020). From the results, it is possible to observe a change in the shock wave position along the stagnation streamline, where the shock position tends to move away from the wall as $a$ increases. A higher value of $a$ increases the forward chemical reaction rate value, thus favoring the endothermic reaction, particularly the dissociation reaction. Higher values of $a$ yield a higher contribution of the translational-rotational temperature mode to the control temperature for the dissociation reactions.

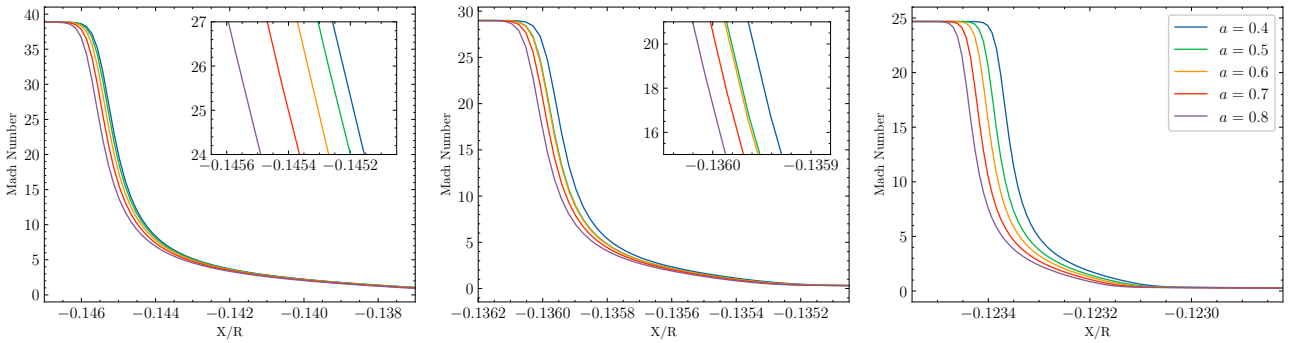


(a) $H = 71.02$ km. (b) $H = 48.37$ km. (c) $H = 41.60$ km.

Figure 2: Mach number distributions at the stagnation streamline.

The translational-rotational temperature mode has higher values than the vibrational-electronic temperature mode, as it is more easily excited (Boyd and Schwartzentruber, 2017). Therefore, the increase in the contribution of the translational-rotational temperature mode on the chemical kinetics of the dissociation reactions leads to a change in the shock wave position. The DSMC method could provide a reference for the shock wave position. However, for the cases studied, the computational cost of running a DSMC simulation in high-density hypersonic flows would not be feasible for this paper.

### 4.3 Temperature Modes and Convective Heat Transfer

Figure 3 shows the temperature mode distributions along the stagnation streamline at the non-equilibrium region. Figures 3(a-b-c) represent the translational-rotational temperature mode and Figs. 3(d-e-f) represent the vibrational-electronic temperature mode. Figures 3(a) and 3(d) are associated with the freestream condition at an altitude of 71.02 km, Figs. 3(b) and 3(e) represent results for conditions at 48.37 km, and Figs. 3(c) and 3(f) represent results for conditions at 41.60 km.

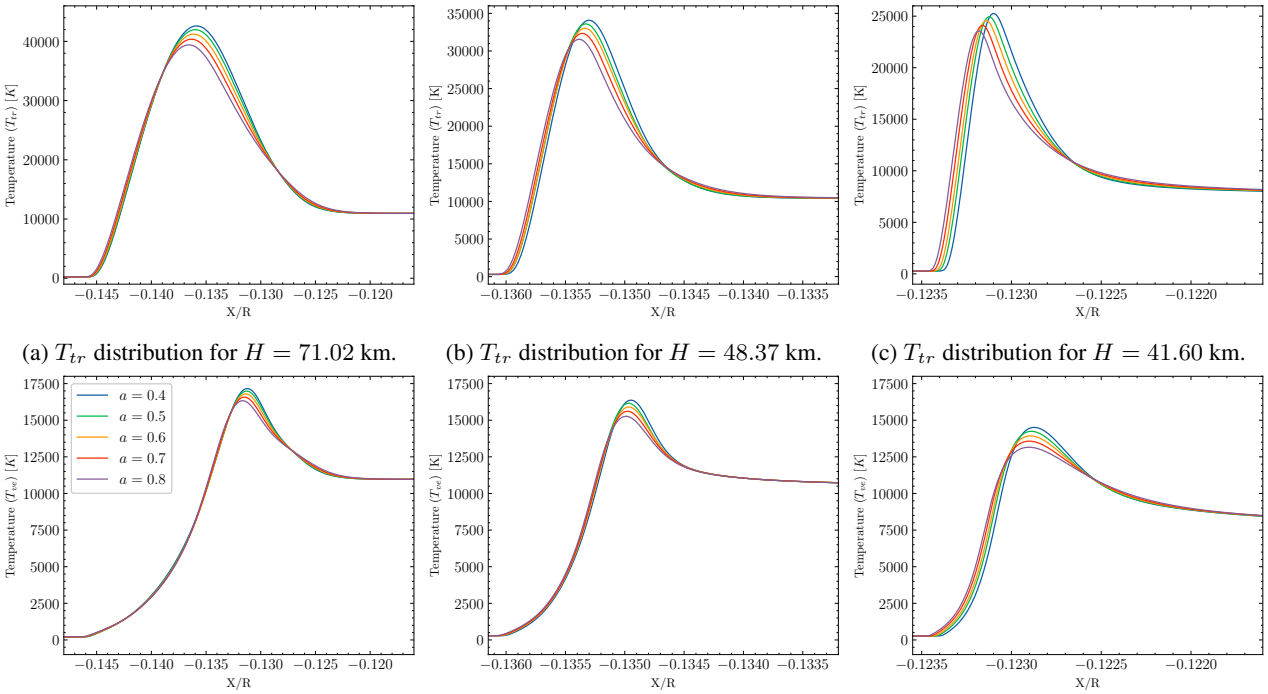


(a) $T_{tr}$ distribution for $H = 71.02$ km. (b) $T_{tr}$ distribution for $H = 48.37$ km. (c) $T_{tr}$ distribution for $H = 41.60$ km.

(d) $T_{ve}$ distribution for $H = 71.02$ km. (e) $T_{ve}$ distribution for $H = 48.37$ km. (f) $T_{ve}$ distribution for $H = 41.60$ km.

Figure 3: Temperature mode distributions in the non-equilibrium region.

The change in the weight factor value causes a difference in the maximum observed value of the temperature modes at the non-equilibrium region for all cases addressed. The increase of $a$ causes a decrease in the maximum values of both temperature modes. The variation can be at a magnitude of thousands of Kelvin. As stated previously, the increase in $a$ makes $T_c$ mainly controlled by the translational-rotational temperature mode, thus affecting the chemical kinetics of the dissociation reactions. The endothermic reactions remove energy from the surroundings to occur. Therefore, less energy goes into the excitation of the different energy modes considered in the present formulation, thus lowering

the temperature modes. The trends observed in the current results show the expected behavior of a system that favors endothermic reactions. In addition, the DSMC method could provide a reference temperature distribution, as presented by Farbar and Boyd (2008). However, the DSMC approach treats the energy modes independently and distributes the energy among them by collisions, while the present work assumes coupled energy modes.

Niu *et al.* (2018) present results for the translational-rotational and vibrational-electronic temperature modes for a blunt body configuration at an altitude of 76 km. However, the reference work uses different body geometries. The freestream Mach number used by the reference is 17.7, which also differs from the ones used in this work. The same authors use the Park two-temperature model with weight factors of $a = 0.5$ and $a = 0.7$. Therefore, the direct comparison of values is not valid, but the behavior of the temperature modes is. With this in mind, the results from this work show the same behavior observed as the reference regarding the vibrational-electronic temperature mode. However, the present results for the translational-rotational temperature mode indicate trends similar to the vibrational-electronic temperature mode. The translational-rotational temperature mode results differ from the behavior presented by Niu *et al.* (2018). Therefore, the geometry and freestream conditions used in the present work may be sufficient to yield the appearance of the influence of the change of $a$ in the translational-rotational temperature mode distribution. This work analyzes cases with higher freestream Mach number values in lower altitudes, which means higher freestream density than Niu *et al.* (2018).

The freestream region and the region between the shock and the capsule thermal shield, except for the non-equilibrium region, show an equilibrium flow behavior. In the equilibrium regions, the different temperature modes tend to have the same value (Bird, 1994; Boyd and Schwartzentruber, 2017). The present work results for the mentioned regions show the expected behavior indicated by the literature, and no significant change is observed in the temperature mode profiles.

Figure 4 shows results for the heat flux at the stagnation point of the flow at the vehicle surface. The results obtained for each test case are close to each other, and their differences are negligible when compared with the magnitude of the heat flux values. Thus, in Fig. 4, there is an overlap of the present computational results for the various values of the weight factor. The differences between the results from the present work and the experimental data are related to the fact that the stagnation heat flux values obtained in the present calculations only consider the convective portion. The experimental data presented have an uncertainty of $\pm 20\%$, represented by the vertical bars. All the results presented are in the error margin of the experimental data.

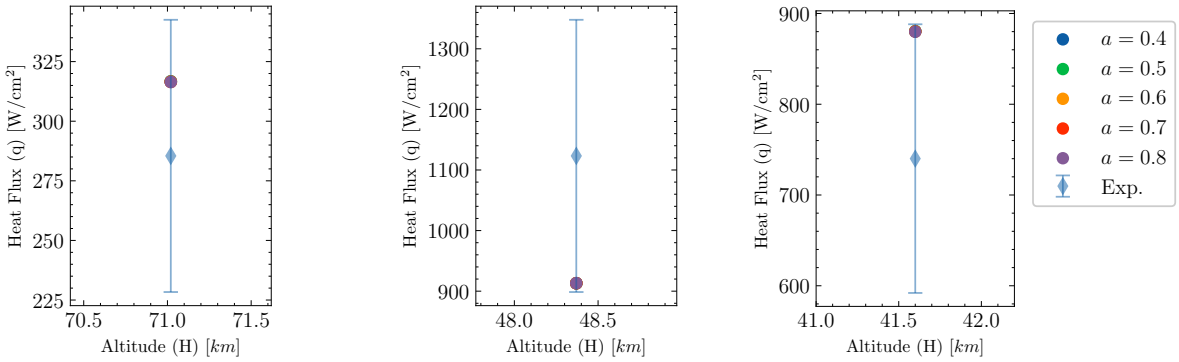


(a) $H = 71.02$ km. (b) $H = 48.37$ km. (c) $H = 41.60$ km.

Figure 4: Heat flux values at the stagnation point.

As stated, the change in $a$ changes the chemical kinetic behavior of the flow, leading to changes in the shock wave position and temperature distribution. In addition, changes occur in the gas mixture composition in the non-equilibrium region. The increase of the weight factor $a$ leads to an increase in the mass fraction of the products of the forward chemical reactions, which are endothermic. These changes could directly affect the estimation of the stagnation point heat flux. However, data from the literature seem to indicate that the primary effect of the mass fraction composition of the chemical species is on the radiative portion of the heat flux (Boyd and Schwartzentruber, 2017). The present work results consider only the convective component of the heat flux, and the results presented in Fig. 4 show that there is no significant change in the convective heat flux at the vehicle's stagnation point with the variation of the $a$ coefficient. The research group has been working on the development of a numerical tool to evaluate the radiative component of the heat flux, which would be directly affected by the variation in the mass fraction of the chemical species present in the mixture. The study of the effects of thermal radiation on non-equilibrium hypersonic flows is outside the scope of this work.

## 5. CONCLUDING REMARKS

This research investigated hypersonic reacting flows under thermodynamic non-equilibrium conditions. The Navier-Stokes equations are solved, including source terms for the chemical reactions occurring in the studied flows. An 11-species model simulates the atmosphere of the Earth. The solver uses a two-temperature model to account for the non-

equilibrium phenomena, using the translational-rotational and vibrational-electronic temperature modes. The present work analyzed the influence of the weight factors of the two-temperature model on the flow behavior. The presented results are in terms of the Mach number and the two temperature modes along the stagnation line. In addition, the present research included results for the heat flux at the stagnation point. This work results indicate good agreement with the literature and experimental data.

The present work analysis aims to obtain data about the influence of the weight factors of the two-temperature model on flow behavior. The results demonstrate that the changes in the weight factors cause changes in the flow behavior in the non-equilibrium region. The shock wave position moves away from the vehicle body as $a$ increases. The maximum temperature observed for both temperature modes in the model tends to decrease as the value of $a$ increases. This behavior is related to the fact that a higher value of $a$ makes the control temperature more influenced by the translational-rotational temperature mode, which typically has a higher magnitude of temperature than the vibrational-electronic mode. This increase in the control temperature value favors the endothermic reactions. The influence of the change in the weight factors over the heat flux at the stagnation point at the vehicle surface was negligible for all test cases analyzed in the present work. The difference between the stagnation heat flux of this work and the experimental data is related to the fact that the formulation used only contemplates the convective portion of the heat flux.

The value of $a$ yields no significative difference to estimate the stagnation point convective heat flux. However, the weight factor value significantly affects the temperature profiles at the non-equilibrium region, especially the maximum temperature values. The present work cannot recommend any values of weight factors for the non-equilibrium region other than those already suggested in the literature. It seems that additional experimental information on property distributions would be necessary in order to provide a better calibration on the values of the weight factors. Nevertheless, the present work has demonstrated that the variations in the property distributions arising from changing the weight factor values are consistent with the expected physical behavior.

## 6. ACKNOWLEDGEMENTS

The authors gratefully acknowledge the support for the present research provided by Coordenação de Aperfeiçoamento de Pessoal de Nível Superior, CAPES, under the Research Scholarship No. 88887.674120/2022-00. The work is also supported by computational resources of the Center for Mathematical Sciences Applied to Industry (CeMEAI), funded by Fundação de Amparo à Pesquisa do Estado de São Paulo, FAPESP, under the Research Grant No. 2013/07375-0. The authors further acknowledge the National Laboratory for Scientific Computing, LNCC/MCTI, Brazil, for providing HPC resources of the SDumont supercomputer, under the HFWBTF project, which have contributed to the research results reported in the present paper. Support to the second author under the FAPESP Scholarship Grants No. 2021/02705-8 and 2022/07604-8, and additional support to the third author under FAPESP Research Grant No. 2013/07375-0 are also gratefully acknowledged. Partial support for the present research was also provided by Conselho Nacional de Desenvolvimento Científico e Tecnológico, CNPq, under the Research Grant No. 309985/2013-7.

## 7. REFERENCES

Agarwal, R.K., Yun, K.Y. and Balakrishnan, R., 2001. "Beyond Navier–Stokes: Burnett Equations for Flows in the Continuum–transition Regime". *Physics of Fluids*, Vol. 13, No. 10, pp. 3061–3085. doi:https://doi.org/10.1063/1.1397256.

Bird, G.A., 1994. *Molecular Gas Dynamics and the Direct Simulation of Gas Flows*. Oxford Engineering Science Series. Oxford University Press, Oxford.

Bird, R.B., Stewart, W.E. and Lightfoot, E.N., 2002. *Transport Phenomena*. John Wiley and Sons, 2nd edition.

Boyd, I.D. and Schwartzentruber, T.E., 2017. *Nonequilibrium Gas Dynamics and Molecular Simulation*. Cambridge Aerospace Series. Cambridge University Press, Cambridge.

Cornette, E.S., 1966. *Forebody Temperatures and Calorimeter Heating Rates Measured During Project FIRE II Reentry at 11.35 Kilometers per Second*. NASA Technical Memorandum, NASA-TM-X-1305. National Aeronautics and Space Administration.

Cramer, M.S., 2012. "Numerical Estimates for the Bulk Viscosity of Ideal Gases". *Physics of Fluids*, Vol. 24, No. 6, pp. 066102.1–066102.23. doi:https://doi.org/10.1063/1.4729611.

Farbar, E. and Boyd, I., 2008. "Simulation of FIRE II Reentry Flow Using the Direct Simulation Monte Carlo Method". In *40th Thermophysics Conference*. American Institute of Aeronautics and Astronautics. doi:10.2514/6.2008-4103.

Gillespie, L.J., 1930. "The Gibbs-Dalton Law of Partial Pressures". *Physical Review*, Vol. 36, No. 1, pp. 121–131. doi:https://doi.org/10.1103/physrev.36.121.

Gnoffo, P., Gupta, R. and Shinn, J., 1989. *Conservation Equations and Physical Models for Hypersonic Air Flows in Thermal and Chemical Nonequilibrium*. NASA Technical Publication, NASA-TP-2867. National Aeronautics and Space Administration.

Hirsch, C., 2007. *Numerical Computation of Internal and External Flows: The Fundamentals of Computational Fluid Dynamics*. Elsevier, Oxford.

Jaeger, F., Matar, O.K. and Müller, E.A., 2018. "Bulk Viscosity of Molecular Fluids". *Journal of Chemical Physics*, Vol. 148, No. 6, pp. 174504.1–174504.12. doi:https://doi.org/10.1063/1.5022752.

Jawahar, P. and Kamath, H., 2000. "A High-Resolution Procedure for Euler and Navier–Stokes Computations on Unstructured Grids". *Journal of Computational Physics*, Vol. 164, No. 1, pp. 165–203. doi: https://doi.org/10.1006/jcph.2000.6596.

Johnston, C.O., Hollis, B.R. and Sutton, K., 2008. "Nonequilibrium Stagnation-Line Radiative Heating for FIRE II". *Journal of Spacecraft and Rockets*, Vol. 45, No. 6, pp. 1185–1195. doi:https://doi.org/10.2514/1.33008.

MacCormack, R.W. and Candler, G.V., 1989. "The Solution of the Navier-Stokes Equations Using Gauss-Seidel Line Relaxation". *Computers and Fluids*, Vol. 17, No. 1, pp. 135–150. doi:https://doi.org/10.1016/0045-7930(89)90012-1.

Martin, A., Scalabrin, L.C. and Boyd, I.D., 2012. "High Performance Modeling of Atmospheric Re-entry Vehicles". *Journal of Physics: Conference Series*, Vol. 341, No. 1, pp. 012002.1–012002.12. doi:https://dx.doi.org/10.1088/1742-6596/341/1/012002.

Moreira, F.C., Wolf, W. and Azevedo, J.L.F., 2021. "Prediction of Hypersonic Reactive Flows During Atmospheric Entry Procedure of the FIRE II Space Capsule". In *Proceedings of the XXVI International Congress of Meschanical Engineering - COBEM 2021*. Brazilian Society of Mechanical Sciences and Engineering, Florianópolis, SC, Brazil.

Moreira, F.C., Wolf, W. and Azevedo, J.L.F., 2023. "Numerical Simulations of Hypersonic Flows over the FIRE II Capsule: Impact of Mesh Resolution and Boundary Conditions on Convective Heat Transfer". In *AIAA SCITECH 2023 Forum*. American Institute of Aeronautics and Astronautics, National Harbor, Prince George's County, Maryland. doi:https://doi.org/10.2514/6.2023-1387.

Moreira, F.C., 2020. *Análise de Escoamentos Hipersônicos em Condições de Não-Equilíbrio Termodinâmico com Aplicações em Reentrada Atmosférica*. Ph.D. thesis, Faculdade de Engenharia Mecânica, Universidade Estadual de Campinas, Campinas, São Paulo.

Niu, Q., Yuan, Z., Dong, S. and Tan, H., 2018. "Assessment of Nonequilibrium Air-chemistry Models on Species Formation in Hypersonic Layer". *International Journal of Heat and Mass Transfer*, Vol. 165, pp. 703–716. doi: https://doi.org/10.1016/j.ijheatmasstransfer.2018.07.007.

Park, C., 1988. "Assessment of a Two-Temperature Kinetic Model for Dissociating and Weakly Ionizing Nitrogen". *Journal of Thermophysics and Heat Transfer*, Vol. 2, No. 1, pp. 8–16. doi:https://doi.org/10.2514/3.55.

Park, C., 1989. "Assessment of Two-Temperature Kinetic Model for Ionizing Air". *Journal of Thermophysics and Heat Transfer*, Vol. 3, No. 3, pp. 233–244. doi:https://doi.org/10.2514/3.28771.

Park, C., 1993. "Review of Chemical-kinetic Problems of Future NASA Missions. I - Earth Entries". *Journal of Thermophysics and Heat Transfer*, Vol. 7, No. 3, pp. 385–398. doi:https://doi.org/10.2514/3.431.

Park, C., 2010. "The Limits of Two-Temperature Kinetic Model in Air". In *48th AIAA Aerospace Sciences Meeting Including the New Horizons Forum and Aerospace Exposition*. American Institute of Aeronautics and Astronautics, Orlando, Florida. doi:https://doi.org/10.2514/6.2010-911.

Scalabrin, L.C., 2007. *Numerical Simulation of Weakly Ionized Hypersonic Flow Over Reentry Capsules*. Ph.D. thesis, University of Michigan, Ann Arbor, Michigan.

Sharma, B. and Kumar, R., 2019. "Estimation of Bulk Viscosity of Dilute Gases Using a Nonequilibrium Molecular Dynamics Approach". *Physical Review E*, Vol. 100, No. 1, pp. 013309.1–0.13309.15. doi: https://doi.org/10.1103/PhysRevE.100.013309.

Steger, J.L. and Warming, R., 1981. "Flux Vector Splitting of the Inviscid Gasdynamic Equations with Application to Finite-Difference Methods". *Journal of Computational Physics*, Vol. 40, No. 2, pp. 263–293. doi: https://doi.org/10.1016/0021-9991(81)90210-2.

Venkatakrishnan, V., 1995. *Implicit Schemes and Parallel Computing in Unstructured Grid CFD*. NASA Contractor Report, NASA-CR-195071. National Aeronautics and Space Administration.

Vincenti, W.G. and Kruger, C.H., 1982. *Introduction to Physical Gas Dynamics*. John Wiley and Sons, New York.

Wilke, C.R., 1950. "A Viscosity Equation for Gas Mixtures". *The Journal of Chemical Physics*, Vol. 18, No. 4, pp. 517–519. doi:https://doi.org/10.1063/1.1747673.

## 8. RESPONSIBILITY NOTICE

The authors are solely responsible for the printed material included in this paper.